Investigating the impact of exopolysaccharides on yogurt network mechanics and syneresis through quantitative microstructural analysis

Food Hydrocolloids 150 (2024) 109629

Contents lists available at ScienceDirect

Food Hydrocolloids

journal homepage: www.elsevier.com/locate/foodhyd

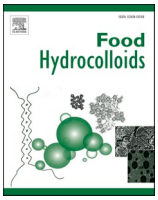

Investigating the impact of exopolysaccharides on yogurt network mechanics and syneresis through quantitative microstructural analysis

Mariska Brüls [a,b,1], Sanam Foroutanparsa [a,b,1], C. Elizabeth P. Maljaars [c], Maurien Olsthoorn [c], Roderick P. Tas [a,b], Ilja K. Voets [a,b,*]

[a] Laboratory of Self-Organizing Soft Matter, Department of Chemical Engineering and Chemistry, the Netherlands
[b] Institute for Complex Molecular Systems, Eindhoven University of Technology, P.O. Box 513, 5600 MB, Eindhoven, the Netherlands
[c] DSM Biotechnology Center, Alexander Fleminglaan 1, 2613 AX, Delft, the Netherlands

ARTICLE INFO

Keywords:
Stimulated emission depletion microscopy
Quantitative image analysis
Syneresis
Yogurt
Exopolysaccharides
Casein

ABSTRACT

Exopolysaccharides produced by lactic acid bacteria are widely used to improve the sensory properties of yogurt. The relation between the physical properties of the microbial exopolysaccharides and the structural and rheological properties of the yogurt are incompletely understood to date. To address this knowledge gap, we studied how two distinct exopolysaccharides influence the microstructure, rheological properties, and syneresis of yogurt. The effect of a negatively charged, capsular exopolysaccharide produced by *Streptococcus thermophilus* and a neutral, non-capsular exopolysaccharide produced by *Lactococcus lactis* were investigated. Using quantitative microstructural analysis, we examined yogurt samples prepared with either the capsular or the non-capsular exopolysaccharide, and with mixtures of the two. Confocal laser scanning microscopy and stimulated emission depletion microscopy were employed to visualize the microstructures, revealing differences in pore size distribution, protein domain size, and casein interconnectivity that were not apparent through visual inspection alone. Additionally, variations in rheological properties were observed among the different yogurt types. In the yogurt fermented with both bacterial strains, we observed a combined impact of the two exopolysaccharide types on relevant microstructural and rheological properties. The negatively charged capsular exopolysaccharide enhanced casein interconnectivity and gel stiffness, while the neutral non-capsular exopolysaccharide led to thicker protein domains, an abundance of small pores, and a lower loss tangent. These factors collectively hindered syneresis, resulting in improved structural integrity. Our study not only provides valuable insights into the influence of different exopolysaccharides on yogurt properties, but also presents the first demonstration and quantification of the effect of multiple types of exopolysaccharides on casein interconnectivity. These findings offer guidance for the production of yogurts with customized microstructure, rheological properties, and resistance to syneresis.

1. Introduction

Yogurt is a widely consumed dairy product that is made by fermenting milk with lactic acid bacteria (LAB). During yogurt production, lactic acid bacteria convert lactose into lactic acid, which causes the milk to acidify. Casein micelles, which constitute 80% of the total milk protein, begin to aggregate into a gel network once the pH drops below their isoelectric point of 4.6 (Lee and Lucey, 2010). The casein micelles are assemblies of multiple casein proteins, including αs_1-, β-, αs_2-, and κ-casein, and colloidal calcium phosphate (Lucey, 2002). During acidification, the caseins rearrange into a particulate gel network that is mainly held together through non-covalent hydrophobic interactions (Horne, 1998). Furthermore, prior to acidification, when heat-induced denaturation occurs, the remaining 20% of milk proteins, known as whey proteins, become covalently bound to κ-caseins. This process leads to the reinforcement of the casein network (Lucey et al., 1998).

A freshly formed yogurt network can still undergo changes due to the relaxation of non-covalent intermolecular bonds, which allow the caseins within gel strands to rearrange. Additionally, strands can break as a result of internal stress induced by thermal motion (van Vliet, van Dijk,

* Corresponding author. Laboratory of Self-Organizing Soft Matter, Department of Chemical Engineering and Chemistry, the Netherlands.
E-mail address: i.voets@tue.nl (I.K. Voets).
[1] shared first co-authorship.

https://doi.org/10.1016/j.foodhyd.2023.109629
Received 27 September 2023; Received in revised form 23 November 2023; Accepted 5 December 2023
Available online 9 December 2023

Zoon, & Walstra, 1991). The relative proportion, strength and relaxation time of the protein-protein bonds (Roefs, De Groot-Mostert, & Van Vliet, 1990), along with the evolving network dynamics, have a significant impact on the thickness and connectivity of gel strands (Van den Bijgaart, 1988). These factors, in turn, affect the loss modulus (G''), storage modulus (G'), loss tangent and syneresis of a yogurt. For example, thicker protein strands in milk gels have been associated with improved resistance to structural rearrangements and higher yield stress (Hussain, Grandison, & Bell, 2012). Lee & Lucey observed that syneresis in yogurt is positively correlated with loss tangent ($r = 0.63$) and negatively with storage modulus ($r = -0.66$) (Lee & Lucey, 2003). Restricting the interactions between casein micelles by enzymatic-crosslinking of caseins within micelles (Nieuwland, Bouwman, Bennink, Silletti, & de Jongh, 2015) prior to acidification, resulted in a yogurt with lower storage modulus. Conversely, increasing the concentration of caseins in milk enhanced the storage modulus of the final gel. Exopolysaccharides produced by bacteria within yogurt may also impact rheological properties and syneresis, directly as viscosity modifiers, or indirectly through their impact on protein-protein interactions.

Physical properties such as mouth-feel and the absence of whey separation are crucial factors that affect consumer perception (Lee and Lucey, 2010). These properties depend on the microstructural features of the yogurt, which can be altered by modifying the ingredient composition (Aguilera, 2005). To enhance yogurt in a natural and cost-effective manner, many consumers prefer natural and clean-label ingredients, avoiding thickeners and gelling agents (Modler & Kalab, 1983a; Teggatz & Morris, 1990). One approach to improve yogurt properties naturally is to use lactic acid bacteria that produce exopolysaccharides (EPSs). EPSs are bacterial polysaccharides that can either be attached to cells (capsular EPS or cEPS) (Hassan et al., 1996), or secreted into the extracellular medium (free EPS or fEPS) (Cerning, 1990). EPSs may act as immunomodulators (Rajoka et al., 2022) and can significantly affect yogurt microstructure and, consequently, its macroscopic properties. There is a large variety in EPS properties produced by different lactic acid bacteria, and their impact on yogurt sensory properties is not entirely understood. EPS differ in monosaccharide composition, charge density, branching, substitutions, and whether there are entirely excreted or remain attached to the cell wall (Riaz Rajoka, Wu, Mehwish, Bansal, & Zhao, 2020). While some EPSs enhance desired properties such as improved viscosity and mouthfeel (Amatayakul, Halmos, Sherkat, & Shah, 2006; Ruas-Madiedo, Alting, & Zoon, 2005), others may cause undesirable side effects, such as excessive ropiness (Mende, Rohm, & Jaros, 2016).

Extensive research has been dedicated to investigating the relation between the rearrangements of casein micelles and their interactions during acidification, which ultimately lead to casein aggregation. Additionally, there exist a comprehensive understanding of network microstructure and mechanics in this context. However, the relationship between these phenomena and EPS type is not well understood yet due to the complexity of fermented yogurt. EPS can affect the formation of the three-dimensional porous protein network that forms when milk acidifies (Harwalkar & Kalab, 1986; Modler & Kalab, 1983b). When yogurt is made with EPS-producing LAB, the EPS concentration gradually increases during fermentation. Depending on the properties of the EPS, such as charge density, it can either interact with the proteins or reside within the pores of the gel network. Different types of EPS can impact the network through distinct pathways, making it challenging to pinpoint the precise effects. Therefore, a systematic and quantitative analytical method is needed to study the effect of EPS characteristics on yogurt microstructure and mechanical properties. Previous research has demonstrated that the viscosity of EPS is influenced by its stiffness, molecular mass (Faber, Zoon, Kamerling, & Vliegenthart, 1998; Kleerebezem et al., 1999), localization in the network (Hassan et al., 2002) and charge (Hassan, 2008). These characteristics primarily determine how EPS affects the microstructure and mechanical properties of the network. Moreover, electron and fluorescence microscopy imaging of yogurt containing EPS has revealed its impact on pore size (Hassan et al., 2003) and network compactness (Hassan et al., 2002). However, we still lack a comprehensive visualization of the microstructures of dairy gels fermented with different LAB strains and the (re)distribution and connectivity of the αs_1-and β-caseins at sub-micrometer length scales within such fermented yogurt, which is important to fully understand how EPS producing LAB impact network microstructure, rheological properties and syneresis.

Fluorescence microscopy is a powerful technique that enables direct visualization of protein networks stained with fluorescent dyes (Arltoft et al., 2007a; Arltoft et al., 2007b; Laneuville & Turgeon, 2014; Zhang, Folkenberg, Qvist, & Ipsen, 2015, 2016). When combined with quantitative image analysis, confocal microscopy, a laser scanning microscopy (LSM) with a resolution of approximately 200 nm, can provide valuable information at the microscale and identify key characteristics of the protein network (Auty, Twomey, Guinee, & Mulvihill, 2001). Grayscale morphology analysis can be used to measure characteristic parameters such as the pore size (Fenoul et al., 2008) and typical aggregate size (Silva, Legland, Cauty, Kolotuev, & Floury, 2015). Autocorrelation-based image analysis (Glover et al., 2019) is useful for determining the typical length of protein domains. Super-resolution microscopy techniques, such as stimulated emission depletion (STED) microscopy, offer improved resolution down to 50 nm, allowing visualization of submicron-scale variations in structure and composition that were previously impossible to observe. STED is an LSM equipped with a doughnut-shaped depletion laser that is aligned with the excitation laser and depletes the fluorophores in the overlapping region (Hell & Wichmann, 1994). This technology holds great promise for revealing the fine details of protein networks and their interactions.

In this study, we examined the microstructure of yogurt fermented with either a *Streptococcus thermophilus* strain, a *Lactococcus lactis* strain or with both. The *Streptococcus thermophilus* strain produces capsular, negatively charged EPS ($cEPS^-$). The *Lactococcus lactis* strain produces a free, neutral EPS ($fEPS^0$). To visualize the protein networks within the yogurt, we labeled the proteins non-covalently with Rhodamine B and used confocal microscopy to image the network structure. We analyzed these images to measure the average protein domain size, pore size distribution, and pore fraction of the fermented yogurt. We also studied the spatial distribution of αs_1-and β-caseins in fermented yogurt STED microscopy, using specific antibodies raised against these proteins. To examine the microstructural connectivity of caseins within the protein network and to quantify the link density (LD), we performed skeleton analysis on the STED images (Foroutanparsa, Brüls, Maljaars, Tas, & Voets, 2023). To explore the relationship between network microstructure and macroscopic properties, we measured the rheological characteristics through oscillatory shear measurements. We also measured whey separation due to gel shrinkage in the absence of an applied force (endogenous syneresis). By combining confocal and STED microscopy, we were able to relate the structural characteristics measured at the microlevel and αs_1-and β-casein distribution at sub-microlevel to variations in mechanical properties. Interestingly, while the yogurt fermented with both bacterial strains showed reduced syneresis compared to yogurt fermented with only one of the strains, its rheological and microstructural properties resembled those of either the $cEPS^-$ and $fEPS^0$ containing yogurt, respectively. This knowledge can help to select bacterial cultures or optimize process conditions to induce desired properties in yogurt.

2. Materials and methods

2.1. Materials

Two lactic acid bacterial strains, one *Streptococcus thermophilus* strain producing anionic capsular polysaccharide ($cEPS^-$) and the other a *Lactococcus lactis* strain producing neutral free EPS ($fEPS^0$), and yeast extract were kindly provided by DSM (Delft, The Netherlands). The

exact strain names are confidential information for this company and cannot be disclosed. Fresh pasteurized skimmed milk (fat content <0.1%, de Zaanse Hoeve) was locally purchased in the Netherlands. Rabbit anti-bovine β-casein polyclonal antibody (ref. BS-10032R) and rabbit anti-bovine αs_1-casein polyclonal antibody (ref. BS-10033R) were obtained from Bioss Inc, U.S.A. Rhodamine B, poly-L-lysine (ref. P8920), phosphate buffer tablets, ATTO647N–NHS ester (ref. 94822) were purchased from Sigma-Aldrich, Merck Life Science NV, The Netherlands. Paraformaldehyde 32% Aqueous solution (EM GRADE, ref. 15714) was obtained from Electron Microscopy sciences, Hatfield, U.S.A. All compounds were used as received.

2.2. Confocal laser-scanning microscopy

2.2.1. Yogurt fermentation

Fresh pasteurized skimmed milk was heated in a thermomixer (Eppendorf® ThermoMixer® C) with mild agitation (300 rpm) for 15 min at 90 °C, followed by 30 min at 85 °C. To ensure optimal growth for $cEPS^-$ producing bacteria, 1% yeast extract was added prior to heating. The $fEPS^0$ producing bacteria do not require yeast extract for optimal growth. The heat-treated milk was cooled down at room temperature (RT) for 1 h and stored overnight at 4 °C. The next day sodium formate (5 mg/ml) and Rhodamine B (0.1 μg/ml) was added to both batches. The milk was heated to 37 °C and after 30 min the milk was inoculated with $cEPS^-$ producing *Lactococcus lactis* strain, $fEPS^0$ producing *Streptococcus thermophilus* strain or a combination of both. Inoculum concentrations were chosen such that the fermented milk reaches pH 5 after 5 h so that all yogurts have similar acidification rates (Supplementary Fig. S1). To accomplish this, the $cEPS^-$ and $fEPS^0$ bacterial strains were diluted to OD_{600} of 1.35 and 0.73, respectively. Subsequently, the dilutions were used to inoculate milk at a ratio of 1:20. For preparing the yogurt with combination of both strains, milk containing 1% yeast extract was inoculated with the same dilutions of bacterial strains at a ratio of 0.5: 0.5: 20.

2.2.2. Sample preparation for confocal imaging

For confocal microscopy of the intact protein network, rhodamine B at a final concentration of 0.1 μg/ml was added to the heat-treated milk. The stained milk was then inoculated as described above and quickly transferred to a chambered microscopy slide (chamber volume = 500 μl) equipped with integrated heating element (VaHeat, Interherence) that maintained the sample temperature at 37 °C. For every system, yogurt fermentation was performed 5 times. Each of these repetitions is referred to as a sample. After fermentation for 8 h, ten images per sample were directly taken of the final network structure at random locations, resulting in a total of 50 images per system. The experiment was repeated with an additional ageing step after the fermentation, with again 5 repetitions and 10 images per repetition at random locations. In this case, samples were stored at 4 °C for one day prior to imaging.

2.2.3. Confocal microscopy

Confocal laser-scanning microscopy (CLSM, Leica SP8) was performed in inverted mode with a 100x oil-immersion objective. The pixel size was set to 80 nm, using 0.75 digital zoom to generate images of 1936 × 1936 pixels. Samples were excited with an incident laser at 552 nm with detection between 565 and 630 nm. All images were taken >10 μm above the glass/yogurt interface to avoid boundary anomalies in the gel formation (Glover et al., 2019).

2.2.4. Quantitative data analysis of CLSM images

2.2.4.1. Pore fraction analysis. The CLSM images are quantitatively analyzed using pore fraction analysis and autocorrelation analysis to differentiate between samples of different systems. To enhance the contrast, the images were rescaled using the automatic brightness adjustment function in ImageJ prior to analysis. The analysis was performed using Python 2 with built-in functions for area calculation, Fourier transformation, and customized functions. To calculate the pore fraction, a Wiener smoothing filter of 5 × 5 pixels was applied to the images using the 'Wiener' function in SciPy. Following the approach of Pugnaloni et al. (Pugnaloni, Matia-Merino, & Dickinson, 2005), the images were thresholded and converted into 8-bit binary images, with the mean grey level as the threshold. Pixels with grey levels above the mean value were considered part of the protein network, and those with grey levels below were considered part of the voids within the network. The pore fraction was calculated as the total pore area divided by the total image area.

2.2.4.2. Autocorrelation analysis. The autocorrelation analysis were performed using the method described by Glover et al. (Glover et al., 2019). The autocorrelation *G(a,b)* of an image is defined as:

$$G(a,b) = \sum_{x=1}^{M}\sum_{y=1}^{N} I(x,y) \bullet I(x-a, y-b) \tag{1}$$

where M and N are the number of pixels in the height and width of the image, *(a,b)* are the coordinates in the generated autocorrelation image, *I(x,y)* is the intensity value of the pixel at *(x,y)*, and μ is the mean intensity of the image. To compute the autocorrelation image efficiently, we used the Wiener-Khinchin theorem (Robertson, 2012), which states that the autocorrelation function is the inverse Fourier transform of the power spectrum image:

$$S(I) = |\mathscr{F}[I(x,y)]|^2 \tag{2}$$

$$G(a,b) = \mathscr{F}^{-1}[S(I)] \tag{3}$$

Where *S(I)* is the power spectrum of the image, $\mathscr{F}$ represents the Fourier transform and $\mathscr{F}^{-1}$ the inverse of the Fourier transform. The power spectrum describes how the signal is distributed over the spatial frequencies that together form the image. To reduce the influence of variations in intensity over the samples, we computed a normalized autocorrelation $g(a,b)$, which is computed by subtraction of the mean intensity, and division by the standard deviation of the image:

$$g(a,b) = \frac{1}{\sigma(x,y)^2}\mathscr{F}^{-1}[\mathscr{F}[I(x,y) - \langle I(x,y)\rangle] \bullet \mathscr{F}^{*}[I(x,y) - \langle I(x,y)\rangle]] \tag{4}$$

Here, $\sigma(x,y)$ is the standard deviation of the intensity values of the source image I, $\mathscr{F}^{*}$ denotes the complex conjugate of the Fourier transform, and $\langle I(x,y)\rangle$ is the average intensity in the image. We then computed the radial distribution of the autocorrelation and power spectrum images using a custom-built Python function that calculates, for every pixel in the image, the distance to the center of the image and averages the correlation values over the pixels that have the same distance to the center. The radially averaged correlation values were normalized by dividing by the largest value, which is at the image center. The radially averaged autocorrelation decay can be fit to a stretched exponential, as demonstrated by Ako et al. (Ako, Durand, Nicolai, & Becu, 2009):

$$p(r) = C \bullet e^{-\left(\frac{r}{\xi}\right)^{\beta}} \tag{5}$$

Here, C is a constant, β is a value between 1 and 2, and ξ is the characteristic length which in this paper was taken as a measure of the protein domain size. We used the scipy function 'curve_fit' to fit the model *p(r)* to the radial distribution of the autocorrelation image for each microscopy image, and extracted the value for the characteristic length ξ.

2.3. Stimulated emission depletion (STED) microscopy

2.3.1. Sample immobilization and labeling

As described above in section 2.2.1, milk was inoculated with the two bacterial strains to produce three different types of yogurt: one solely fermented with $cEPS^{-}$ producing strain, $fEPS^{0}$ producing strain and a combination of both strains. After 8 h incubation at 37 °C, the fermentation was complete, and the yogurt was immobilized onto a clean microscope slide, which was taped with double-sided adhesive tape. A poly-L-lysine-coated coverslip was placed on top to create a flow chamber containing a turbid yogurt. The sample was incubated inside the chamber upside down at room temperature (RT) for 10 min. For fixation, 25 μl of freshly prepared 4% (w/v) formaldehyde solution in 10 mM phosphate buffer solution (PBS) was injected into the chamber and incubated upside down at RT for another 20 min, as described previously (Berg & Fishman, 2019). The chamber was then rinsed by injecting 200 μl of PBS inside to prepare for staining. To localize β- and αs_1-casein, rabbit anti-bovine β-casein polyclonal antibody and rabbit anti-bovine αs_1-casein polyclonal antibody were labeled with ATTO647N–NHS ester, which is a suitable dye for STED microscopy, following a protocol described earlier (Berg & Fishman, 2019). The dye-conjugated primary antibodies (degree of labeling = 3–4.5 fluorophores per antibody) were diluted to 200 μg/ml, and 25 μl of the solution was injected into the chambers containing yogurt from the same batch and incubated at 4 °C overnight. Following extensive washing with PBS buffer, the chamber was sealed and prepared for STED microscopy. The selectivity of the αs_1-and β-casein antibodies within the acid dairy gel has been confirmed in earlier work (Foroutanparsa, Brüls, Tas, Maljaars, & Voets, 2021).

2.3.2. STED microscopy imaging of fermented yogurt

Super resolution imaging was performed using a STED microscope (Abberior Instrument, Göttingen, Germany) equipped with UPlanSApo 100x/1.40 Oil [infinity]/0.17/FN26.5 objective (Olympus), a Katana-08 HP laser (Onefive) and multiple STED laser lines at 405 nm, 488 nm, 561 nm, 640 nm, as well as a pulsed laser at 595 nm and 775 nm, with aid of Imspector 0.14.13919 software. Typically, the images were acquired with a pixel size of 30 nm and a pixel dwell time of 10 μs. The images were taken approximately 1 μm above the coverslip where the structure was fixed with formaldehyde solution and immobilized to achieve the highest signal-to-noise ratio. A pinhole was set at 1.00 AU at 100x. ATTO647N was excited at 640 nm (5% laser power), while STED was achieved using a wavelength of 775 nm (4% laser power). The obtained 8-bit non-compressed TIFF STED images were exported for further analysis. Single-color images of αs_1-and β-caseins were collected from the same batch of yogurt, and three images were taken of each prepared sample. For every system, yogurt fermentation was performed at least 8 repetitions. Each of these repetitions is referred to as a sample. For every sample, 3 images were acquired at random locations. In total, at least 26 images were taken for the localization of αs_1-and β-caseins per system.

2.3.3. Skeleton analysis of STED images

To quantify and differentiate between the topology of β- and αs_1-casein domains in yogurt gels of different systems, we used a skeleton analysis method. All analysis steps were performed using the Fiji/Image J software (https://imagej.net/software/fiji/). Firstly, we reduced the noise in the 8-bit STED TIFF images by applying a Gaussian filter (radius = 2) and then binarized them using the threshold of "0.9 × mean grey level". The resulting binarized images of protein domains were skeletonized using the Fiji skeleton plugin to produce a one-pixel-wide representative image (Lee, 1994). We then analyzed the skeletonized images, which consisted of a network of branches, using the AnalyzeSkeleton plugin (Arganda-Carreras, Fernández-González, Muñoz-Barrutia, & Ortiz-De-Solorzano, 2010). AnalyzeSkeleton classifies the pixels within the thinned protein domains based on their 26 neighboring positions into three categories: end-point pixels, which have fewer than 2 neighbors; junction pixels with more than 2 neighbors; and slab pixels, which have exactly 2 neighbors. Slab pixels are the building blocks of branches that connect end and junction points. Additionally, we pruned possible loops by cutting the loop branches from their darkest pixel, using the "lowest intensity voxel" as the prune cycle method.

To accurately determine the connectivity of the skeleton, we aimed to identify any dangling ends or loop defects within the network (Supplementary Fig. S2). We utilized the "Prune Ends" option of the plugin to eliminate any branches that were connecting to end points, thus discarding any dangling ends. Additionally, any branches with a Euclidean distance of less than 100 nm (approximately two times the resolution of STED microscopy) were defined as dangling loops and were also removed. To identify the space-spanning network, we identified the skeletons with exclusively branches with Euclidean distances higher than 100 nm. Any other branches that were within finite-size clusters were then removed. By doing this, we were able to obtain the link density, a metric that helps assess the connectivity of the network. We calculated this by taking the total number of linking branches (excluding any dangling ends, loops, and finite-size clusters) and dividing it by the total number of branches. Furthermore, to provide a more comprehensive understanding of the network and its connectivity, AnalyzeSkeleton was used to provide information on the total length of branches per skeleton that was identified within the field of view.

2.4. Rheology

To evaluate the rheological properties of the yogurt systems, a rheometer (Anton Paar GmbH, MCR501) with double gap cylinder geometry (DG26.7-SN188610) was used. After the yogurt was formed, 3.8 ml of the sample was added to the rheometer, along with a few oil droplets to prevent evaporation. The storage modulus G" and loss modulus G′ of the yogurt were determined using the rheometer's oscillatory mode. The loss tangent (tan(δ) is calculated using the formula tan (δ) = G"/G'. A frequency sweep ranging from 100 to 0.1 Hz was performed at a constant amplitude of 1%, and an amplitude sweep ranging from 1 to 10% was taken at a constant frequency of 1 Hz. Each of the three yogurt systems (with either *Lactococcus lactis*, *Streptococcus thermophilus*, or both) was prepared three times and every prepared sample was measured once. The results are presented as the average of these three rheology measurements.

2.5. Endogenous syneresis measurements

To measure the extent of endogenous syneresis, we used a technique described earlier (Lucey, Munro, & Singh, 1998). Skim milk was inoculated with bacteria, as described previously, and 100 g of the resulting mixture was placed in 100 ml plastic cups. The cups were then incubated in a water bath at 37 °C (Supplementary Fig. S3). After 8 h of incubation, the cups were transferred to a refrigerator set at 4 °C. To quantify the endogenous syneresis, the free serum was isolated by pipetting without applying force to the curd. The isolated serum was then measured after 1 h and 20 h (1 day) of storage of the yogurt at 4 °C. The extent of syneresis was reported as a percentage of free serum in the total yogurt sample. Syneresis experiments were conducted in duplicate to ensure the accuracy and reliability of the results.

2.6. Statistical analysis

To analyze the data, we first performed normality tests using the Shapiro-Wilk test and Normal Q-Q plot. The results showed that only the protein domain size distribution in fresh fermented yogurt was normal. Therefore, we used analysis of variance (ANOVA) with Tuckey's test to compare the statistical differences in protein domain size distributions of fresh fermented yogurt. For the pore fractions in both fresh and stored

yogurt, protein domain size in stored yogurt, and link density distributions of αs_1-and β-caseins in fermented yogurt, the Shapiro-Wilk test and Normal Q-Q plot revealed that their distributions were not normal. As a result, we used pairwise non-parametric one-way ANOVA tests (Kruskall-Wallis) to compare the statistical differences in these parameters. All statistical analyses were performed using Graphpad PRISM software (Graphpad Prism Inc., version 9.5.1) for Mac. Results with a P-value <0.05 were considered statistically significant.

3. Results & discussion

3.1. Microstructure of yogurt fermented with bacterial strains

Exopolysaccharides (EPS), present either freely in the medium or adhered to the bacterial cell wall, can greatly influence the microstructure of yogurt (Mende et al., 2016). To investigate the impact of neutral and negatively charged EPS on fermented yogurt, we conducted fluorescence microscopy experiments on yogurt fermented with either *Streptococcus thermophilus*, which produces a negatively charged, capsular EPS ($cEPS^-$) that remains cell wall bound, or *Lactococcus lactis*, which secretes a neutral EPS ($fEPS^0$), or both cultures. Note that the microstructure of yogurt can vary due to multiple factors, such as EPS production rate, LAB proteolytic activity, and EPS concentration and charge density (Girard & Schaffer-Lequart, 2007; Ruas-Madiedo et al., 2005; Tiwari, Kavitake, Devi, & Halady Shetty, 2021). In the fermented yogurt studied herein, we have purposely adjusted the concentrations of the bacterial strains to achieve a comparable acidification rate, to investigate the impact of EPS type (capsular vs. free) and charge density (negative vs. neutral) on microstructure while minimizing the influence of other variables, such as dissimilar acidification rate (Lee & Lucey, 2004). We utilized confocal microscopy to capture general features of the protein network in intact yogurt, and high-resolution STED microscopy to study the distribution of caseins in the protein-rich regions of the network (Fig. 1).

3.2. Microstructural characteristics from confocal microscopy

Confocal imaging was utilized to visualize the overall network structure of the three yogurt types. The fermentation process took place within a heated chambered microscopy slide to ensure accurate measurements of the undisturbed protein network. To provide a comprehensive view of the protein network, rhodamine B was added to the samples as a general protein staining agent. Subsequently, the images were analyzed in Python to evaluate the protein domain size and pore fraction as indicators of the network structure (Fig. 2). The microstructures of fresh yogurt with bacteria that produce $cEPS^-$, $fEPS^0$ or $cEPS^-$ and $fEPS^0$ still appear rather similar after 8h of fermentation (Fig. 2A). The structures, however, of stored yogurt after 24h of fermentation are clearly distinct (Fig. 2A). Clearly, the structure of yogurt continues to develop after gelation in the presence of both types of lactic acid bacteria.

To reveal subtle differences in microstructure that may be overlooked upon qualitative inspection of the confocal images, and to determine the characteristic size of the protein domains (Fig. 2B) and pore fractions (Fig. 2C), we next performed autocorrelation analysis and computed the pore fractions (see methods section for more information). These quantitative image analysis approaches confirmed the differences observed in the stored samples and additionally revealed that there are also significant differences in the microstructure of fresh samples (Fig. 2B and C). After 8 h of fermentation, the protein domains appear smallest in the presence of exclusively $cEPS^-$ (P-value<0.05), although no significant differences were observed for 24 h after the start of fermentation (Fig. 2B). The mean protein domain size in the fresh and stored yogurt fermented with both $cEPS^-$ and $fEPS^0$ resembles that of the corresponding yogurt with exclusively $fEPS^0$. The characteristic protein domain size decreases upon storage in all cases.

All yogurts were visibly porous systems with overall pore fractions ranging from 0.49 for fresh yogurt with $fEPS^0$ up to 0.6 for stored yogurt with either $fEPS^0$ or $fEPS^0/cEPS^-$ (Fig. 2C). Fresh yogurt contained small pores; none of the contained pores are larger than 600 μm^2 and most (>90%) pores were smaller than 200 μm^2 (Supplementary Fig. S4A). The yogurt with either $fEPS^0$ or $cEPS^-/fEPS^0$ contained slightly more small pores (21% and 10% more pores <50 μm^2, respectively) than networks with $cEPS^-$. The larger size of the bacteria with capsular EPS (1–1.2 μm vs. 0.5–0.6 μm, Supplementary Fig. S5) may contribute to the formation of larger pores in $cEPS^-$ yogurt. Coarsening upon storage in the presence of both EPS types caused an increase in both pore fraction and mean pore size. The large pores in the stored yogurt with

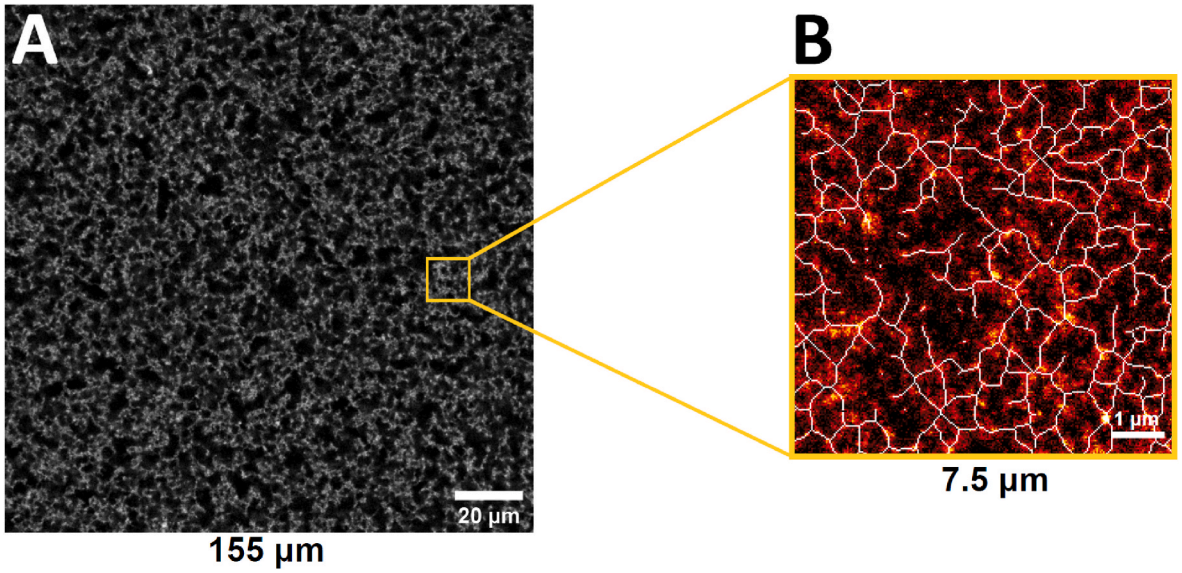

Fig. 1. **(A)** Confocal and **(B)** STED microscopy tools are applied to yoghurt fermented with exclusively $cEPS^-$, $fEPS^0$, or a combination of $cEPS^-$ and $fEPS^0$ to probe **(A)** network microstructure and **(B)** the distribution of caseins in the protein-rich regions of the network. To this end, ±50 regions of interest of **(A)** 155 mm × 155 mm and **(B)** 7.5 mm × 7.5 mm were imaged and analyzed using **(A)** rhodamine B as a non-specific protein stain and **(B)** ATTO647N labeled antibodies against αs_1- and β-casein, respectively. Images were subsequently analyzed using Python and ImageJ plug-in AnalyzeSkeleton to determine microstructural network features, such as protein domain size, pore size (distribution) and casein connectivity.

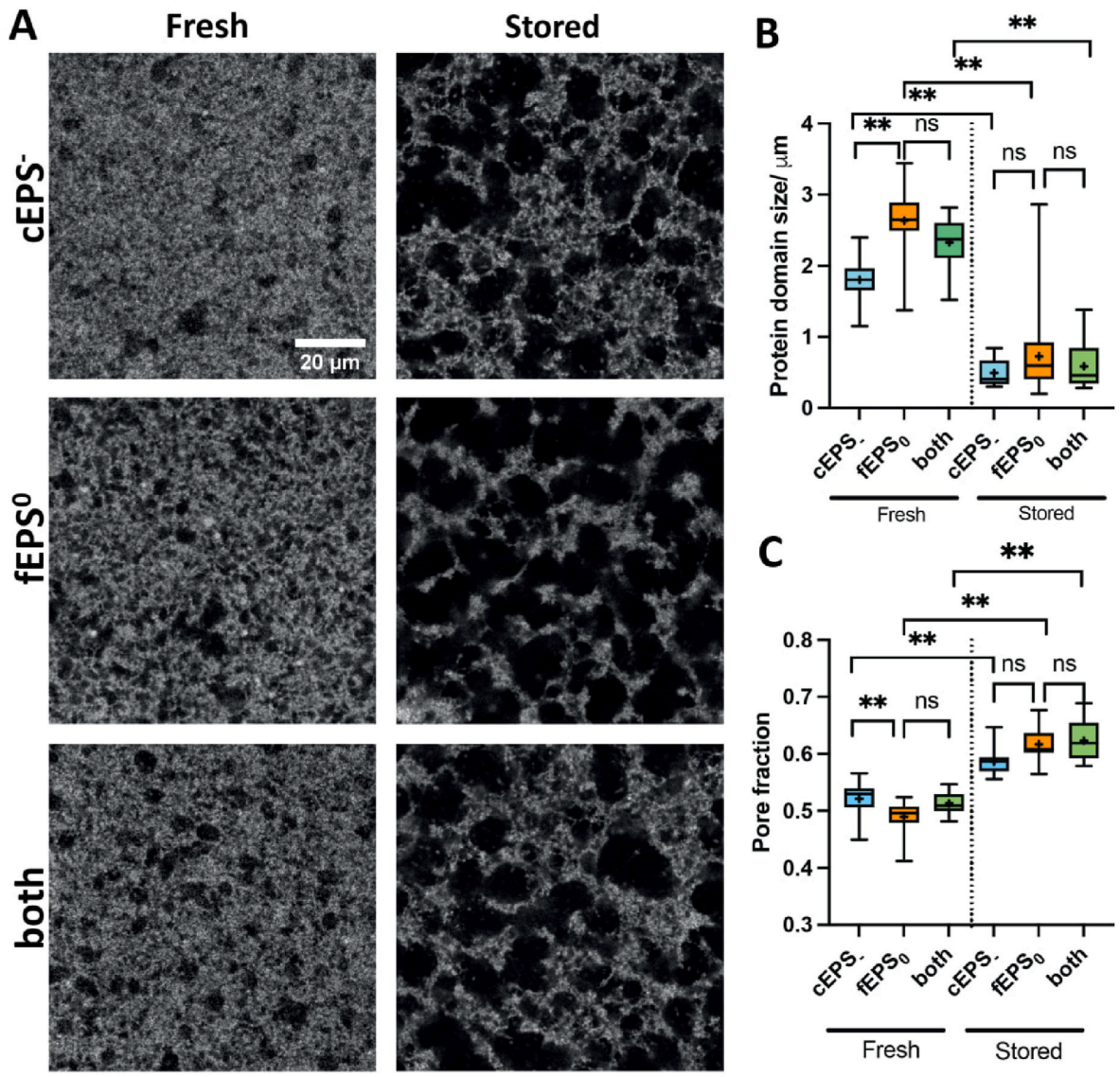

Fig. 2. **(A)** Confocal images of the protein network structures of the fermented yogurt, prepared with bacteria producing cEPS$^-$, fEPS^0 or cEPS$^-$/fEPS^0 mixture. Box plots of the distribution in **(B)** protein domain size, and **(C)** pore fraction of the 50 images taken from every system. For every system, 5 samples were prepared starting from inoculation and 10 images were taken per sample. In the box plot, the whiskers extend from the minimum to the maximum value, the mean of the data is denoted by "+", and the median line is shown.

dimensions exceeding 8000 µm^2 (Supplementary Fig. S4B) correspond to large, interconnected voids in the network. Less than 30% of all pores in these stored samples were smaller than 200 µm^2. The cEPS$^-$ system retained the largest proportion (54%) of pores with <500 µm^2. This may be due to a higher retention of cEPS$^-$ producing LABs within the <500 µm^2 pores due to complexation of the negatively charged, cell-surface attached EPS with the positively charged casein network. We propose that free, uncharged fEPS^0 and fEPS^0 producing LABs interact in a weaker fashion with the casein network, and therefore likely accumulate more readily within the large, interconnected voids.

3.3. *The presence of capsular EPS promotes the formation of highly connected domains of αs_1 and β-caseins*

Simultaneous confocal and STED imaging was next employed to visualize the spatial distribution of αs_1-and β-caseins in the three types of yogurt and assess whether the production of neutral and/or negatively charged EPS during fermentation with one or both of the bacterial strains impacts the microstructures that form. To this end, fresh gels were gently immobilized and treated with 4% (w/v) formaldehyde solution. The samples were subsequently stained with antibodies specific to αs_1-and β-caseins as soon as fermentation was complete, which was after 8 h. Next, we simultaneously acquired confocal laser scanning microscopy (CLSM) and STED images of the protein-rich regions to achieve high resolution and identify potential differences in the distribution of αs_1-and β-caseins and the connectivity of the self-assembled protein domains (Supplementary Fig. S6).

Interconnected networks of both αs_1-and β-caseins are visible in yogurt with either exclusively cEPS$^-$ or both cEPS$^-$ and fEPS^0 (Fig. 3). Both yogurt networks also contained micron-sized voids in the visualized protein-rich regions, some of which are indicated by white arrows in Fig. 3. Such large voids were not found in the yogurt with fEPS^0. Complementary imaging of stored cEPS$^-$ yogurt stained with the amine-reactive ATTO 647N–NHS ester, which binds protein but also the capsular exopolysaccharide, revealed that cEPS$^-$ producing bacteria reside inside the micron-sized pores in the protein-rich domains in these systems (Supplementary Fig. S7).

To determine the connectivity of the αs_1-and β-caseins in the three

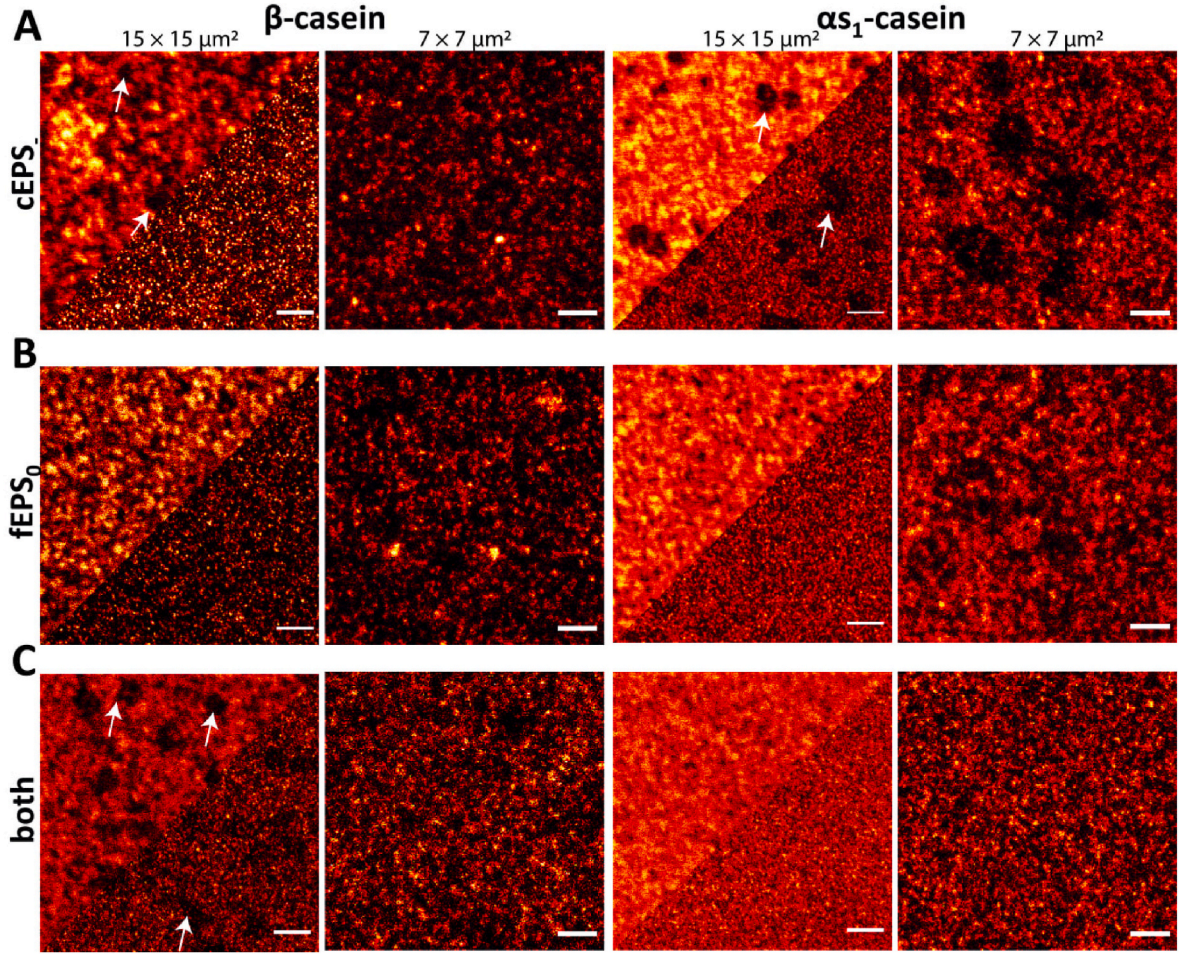

Fig. 3. Simultaneous confocal and STED imaging of αs_1-and β-caseins in the microstructure of fresh yogurt fermented with: **(A)** cEPS$^-$producing LAB (cEPS$^-$), **(B)** fEPS^0 producing LAB (fEPS^0), and **(C)** a mixture of cEPS- and fEPS^0 producing bacteria (cEPS$^-$/fEPS^0). Scale bars in zoomed-out (15 ×15 μm^2) and zoomed-in (7 × 7 μm^2) images are 2 μm and 1 μm, respectively.

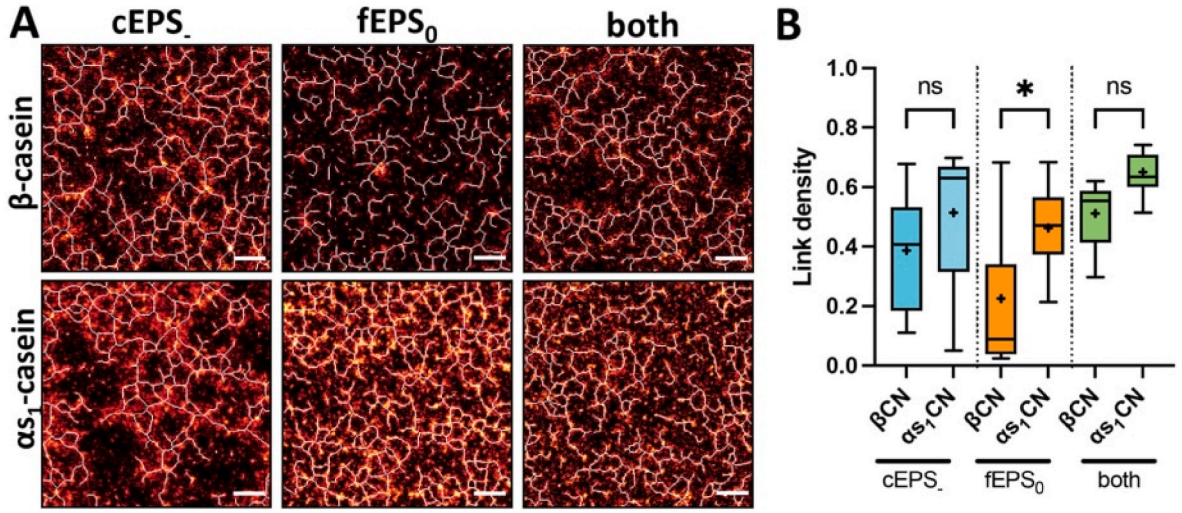

Fig. 4. Skeleton analysis of STED images of αs_1-and β-caseins in the microstructure fresh yogurt. **(A)** an overlay of raw image and skeletonized network for yogurt fermented with cEPS-producing LAB (cEPS$^-$), fEPS-producing LAB (fEPS^0), and combination of both strains (cEPS$^-$/fEPS^0). Scale bars in panel A are 1 μm. **(B)** Distribution of the link densities of αs_1-and β-caseins in fermented yogurt. For every system, at least 8 samples were prepared starting from inoculation, and 3 images were taken per sample. In the box plot, the whiskers extend from the minimum to the maximum value, the mean of the data is denoted by "+", and the median line is shown.

types of fermented yogurt, and identify potential differences in their network architecture that may escape visual inspection, we conducted a skeleton analysis (Doube et al., 2010; Odgaard & Gundersen, 1993) of the STED micrographs (Fig. 4). This allowed us to compute the link density (ρ_{link}) of the skeletonized casein networks (Fig. 4A). The link density (Fig. 4B) is given by the ratio of the number of linking branches (excluding dangling ends, loops, and finite aggregates) to the total number of branches in two-dimensional images of a network (Supplementary Fig. S7). The link density ρ_{link} can thus be taken as an indicator of network connectivity.

A comparison of the determined link densities for the three types of yoghurt reveals that the connectivity of both the αs_1-and β-casein domains, is higher for the two yogurt types that contain the negatively charged capsular EPS (Fig. 4B). Specifically, we determined $\rho_{link,a} = 0.65 \pm 0.06$ and $\rho_{link,b} = 0.51 \pm 0.1$ for cEPS$^-$/fEPS^0 yogurt and $\rho_{link,a} = 0.51 \pm 0.2$ and $\rho_{link,b} = 0.39 \pm 0.2$ for cEPS$^-$ systems, whilst for fEPS^0 yogurt we have $\rho_{link,a} = 0.46 \pm 0.1$ and $\rho_{link,b} = 0.22 \pm 0.2$. Hence, the skeleton analysis indicates that both αs_1-and β-caseins contribute to the connectivity of the fermented dairy gels, and, that the cEPS$^-$ producing strain induces a higher network connectivity than the fEPS^0 producing strain. Tentatively, we propose that networks with the cEPS$^-$ producing strain are more compact and inter-connected, because herein the casein networks can reconfigure more. We further postulate that this is due to a difference in the onset of EPS production, with cEPS$^-$ being produced before the onset of gelation and fEPS^0 being produced after the onset of gelation. We argue that secretion of fEPS^0 into the network pores during the later stages of gelation leads to a relatively modest impact on network reconfiguration and microstructure compared to cEPS$^-$ (Mende et al., 2016), which is presumably produced earlier, likely before the onset of gelation (Hassan, Frank, & Qvist, 2002). It is important to note however that the influence of fEPS^0 on network mechanics may still be significant. For instance, fEPS^0 may enhance the viscosity of the serum within the network pores and increase attractive interactions between caseins due to bridging and/or depletion interactions (Tuinier, ten Grotenhuis, Holt, Timmins, & de Kruif, 1999).

The link density values for all the fermented yogurt types are comparable to the link densities (0.34 ± 0.06 for αs_1-casein and 0.6 ± 0.02 for β-casein) reported previously by us for αs_1-and β-casein structures in GDL-acidified milk protein gels (Supplementary Fig. 8) (Foroutanparsa et al., 2023). Despite the overall similarity in link density, subtle differences are notable. ρ_{link} tends to be higher for αs1-than β-casein domains in all fermented gels (Fig. 4B). By contrast, ρ_{link} was lower for αs_1-than β-domains in the GDL-acidified gels (Foroutanparsa et al., 2023). The reason for this difference is as yet unknown, but we suspect that it has to do with a more pronounced release of β-caseins than of αs_1-caseins from casein micelles in GDL-acidified milk protein gels as determined by ultracentrifugation and electrophoretic gel separation (Dalgleish & Law, 1988). Our results thus confirm earlier observations that GDL acidified gels and fermented milk gels behave differently (Lucey, Munro, & Singh, 1998). This may be due to an interplay of different phenomena, such as the impact of the EPS on casein solubility (Ni & Raikos, 2019) and on the dissociation of caseins from the micelles during the acidification. In addition, acidification rates are different and the proteolytic activity of LAB may play a role (Kunji, 1996).

3.4. Rheological and syneresis properties of yogurt

Next, we examined the mechanical properties of the fermented yogurt. We used oscillatory rheometry to measure the viscoelastic characteristics of the fermented milk gels across a frequency range of 0.1–100 Hz (Fig. 5). The milk gels fermented with fEPS^0 exhibited lower G' and G" compared to the systems with either cEPS$^-$ or cEPS$^-$/fEPS^0 strains (Fig. 5A). Additionally, the loss tangent of cEPS$^-$ yogurt was slightly higher than that of fEPS$_0$ and cEPS$^-$/fEPS^0 yogurt (Fig. 5B).

We also quantified the extent of endogenous syneresis by measuring the weight ratio of whey separated from the curd and the total weight of the yogurt (Fig. 5C). Syneresis was most pronounced in the fresh yogurt. This is because the network can still undergo major reconfigurations during this time as many bonds are transient (Lucey, Munro, & Singh, 1998). Interestingly, we found that the fresh yogurt fermented with a combination of both strains had on average a lower syneresis compared to those fermented with either cEPS$^-$ or fEPS^0 alone, both of which showed on average about twice as much syneresis (Fig. 5C). After 1 day of storage, syneresis notably reduced in all cases. However, the variability in syneresis among the fresh yogurts and among the stored yogurt is too large to confirm any statistically significant difference among the yogurts fermented with different bacterial strains.

3.5. Relation between microstructural characteristics and rheological properties

Having quantified microstructural and rheological features of three types of fermented yoghurts, it is of interest to examine their relation. Subtle differences in network connectivity were identified as variations in link densities determined by a skeleton analysis. The mixed fEPS^0/cEPS$^-$ dairy gels consisted of interconnected αs_1-and β-casein domains with a high link density, similar to the cEPS$^-$ yogurt (Table 1). The storage and loss moduli of these two yogurt types were also larger than those of the fEPS^0 gel. It is likely that the high connectivity of the αs_1-and β-casein domains in the two gels with cEPS$^-$ gives rise to the formation of a stronger viscoelastic material with a higher G′ and G". Based on these findings, the link density seems to be a good indicator for the G′

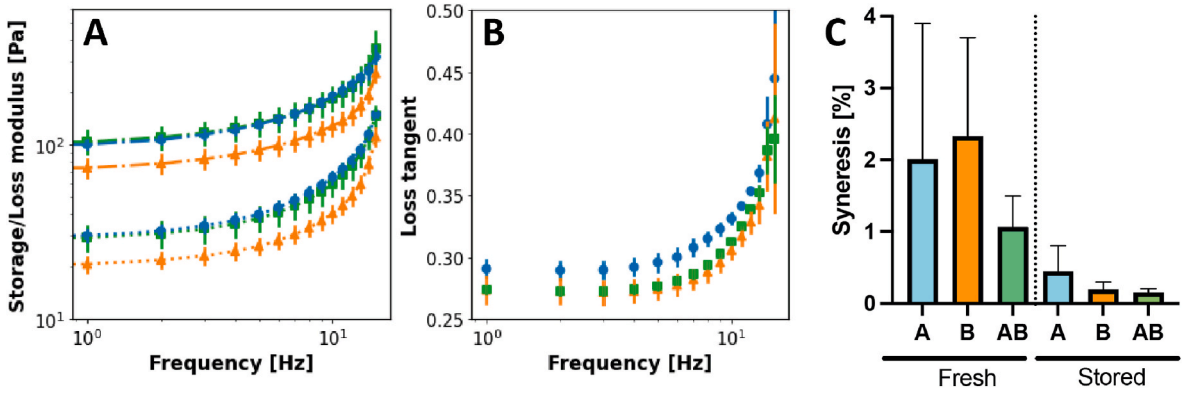

Fig. 5. Mechanical characteristics of fermented yogurt measured by: (**A-B**) oscillatory rheometry of fresh yogurt (**A**) Storage modulus, G' (dash-dotted line), and loss modulus, G'' (dotted line), and (**B**) loss tangent of stored yogurt as a function of frequency for yogurt prepared with cEPS- (blue circles), fEPS^0 (orange triangles) and both strains (green squares). (**C**) Syneresis expressed as percentage of serum separated from in the fresh yogurt and during storage for 1 day. The bar chart represents average values with standard deviation shown as error bars.

Table 1
Microstructural and mechanical properties of fresh yogurt fermented with cEPS$^-$, fEPS^0 and combination of both strains. Values are represented as mean ± standard deviation.

Property	cEPS$^-$	fEPS^0	Both
Protein domain size (μm)	1.8 ± 0.3	2.6 ± 0.4	2.3 ± 0.3
Pore Fraction	0.52 ± 0.03	0.49 ± 0.02	0.51 ± 0.02
Pores <50 μm^2 (%)	67	74	86
Link density, αs_1-casein	0.51 ± 0.2	0.46 ± 0.1	0.65 ± 0.06
Link density, β-casein	0.39 ± 0.2	0.22 ± 0.2	0.51 ± 0.1
G' (Pa), at 1 Hz	131 ± 7	93 ± 11	133 ± 20
G" (Pa), at 1 Hz	40 ± 3	26 ± 3	38 ± 6
Tan δ, at 1 Hz	0.30 ± 0.01	0.28 ± 0.01	0.28 ± 0.003
Syneresis after 1h (%)	2 ± 1.3	2.3 ± 1.1	1 ± 0.5

and G″, although more extensive research is needed to confirm this.

For the yogurt fermented with solely fEPS^0 producing bacteria, the autocorrelation analysis revealed the presence of large protein domains, which are presumably compact and consequentially have a high protein-protein bond density. This would make the strands less prone to rearrangements and deformations. Furthermore, the small pores of the size observed for the fresh fEPS^0 networks hampers gel permeation (Fang, Zhang, & Nishinari, 2021) and the presence of non-adsorbing neutral polysaccharide within the pores increases serum viscosity. Both effects are known to slow down syneresis as they increase the time it takes for the EPS to permeate through and diffuse out of the gel. For syneresis to occur, water molecules, small solutes and large EPS should separate from the gel to maintain osmotic balance (Faers, Choudhury, Lau, Mcallister, & Luckham, 2006). The mixed fEPS^0/cEPS$^-$ networks, on average, exhibit the least syneresis, suggesting that fEPS^0 may potentially mitigate whey separation due to low gel permeability, the presence of small pores, and the existence of relatively thick protein strands in yogurt with fEPS^0. However, conclusive evidence to support this hypothesis was not obtained.

Summarizing, we propose that the yogurt with both strains possesses improved rheological properties which can be attributed to the combination of microstructural traits resulting from the action of both bacterial strains. We speculate that yogurt made of combined strains can resist rearrangement better and shows comparatively less syneresis owing to its high degree of casein interconnectivity, combined with larger protein domains and a high number density of small sized serum pores containing non-adsorbing polysaccharides.

4. Conclusion

In conclusion, our multiscale characterization revealed the effects of EPS on the microstructure, rheological properties and syneresis of yogurt fermented with different lactic acid bacterial strains producing either a free, neutral EPS (fEPS^0) or a negatively charged, capsular EPS (cEPS$^-$). Confocal images of the network structure appeared similar upon first inspection, but quantitative image analysis revealed subtle yet statistically relevant differences in protein domain size, pore fraction, and pore size distribution. The yogurt with fEPS^0 and fEPS^0/cEPS$^-$ contained the largest protein domains. STED revealed a high level of connectivity for both the αs_1-and β-casein domains in the cEPS$^-$ and fEPS^0/cEPS$^-$ systems. The β-casein domains in fEPS^0 yogurt were less connected. The yogurt types also differed in rheological properties. The cEPS$^-$ and cEPS$^-$/fEPS^0 yogurt types exhibited a higher storage and loss modulus compared to fEPS^0 yogurt. The presence of cEPS$^-$ appears to promote high connectivity, while fEPS^0 tends to generate networks with large protein domains and small pores. We tentatively relate the modest syneresis in yogurt with both EPS types to the highly connected nature of the casein network and the presence of large protein domains and small pores.

Recent advances in adaptive optics to address refractive index mismatches and improve imaging quality (Jabermoradi, Yang, Gobes, Van Duynhoven, & Hohlbein, 2022; Urban, Willig, Hell, & Nägerl, 2011) can be exploited to extend the present work to high-resolution, 3D imaging of fermented milk gels. It would be of great interest to implement this technological development to take a closer look at the impact of various types of bacterial cultures on fresh and matured casein networks over time and at various concentrations (i.e., resulting in variations in acidification rates). The bioactivity of yogurts with different combinations of exopolysaccharides is also interesting to investigate. Herein we focused on two important bacterial strains that produce different types of EPS. However, not all relevant lactic acid bacterial strains produce EPS. Comparing and contrasting the impact of these different types of LAB on network properties would further advance our understanding of the mechanisms through which LABs and the EPS they produce adapt the structural and functional features of fermented dairy gels. This knowledge can inform the food industry's selection and development of LAB strains to produce yogurt with desired texture and quality.

CRediT authorship contribution statement

Mariska Brüls: Conceptualization, Formal analysis, Investigation, Software, Validation, Writing – original draft. **Sanam Foroutanparsa:** Conceptualization, Formal analysis, Investigation, Software, Validation, Visualization, Writing – original draft. **C. Elizabeth P. Maljaars:** Conceptualization. **Maurien Olsthoorn:** Conceptualization. **Roderick P. Tas:** Conceptualization, Supervision, Writing – review & editing. **Ilja K. Voets:** Conceptualization, Funding acquisition, Supervision, Writing – review & editing.

Declaration of competing interest

The authors declare that they have no known competing financial interests or personal relationships that could have appeared to influence the work reported in this paper.

Data availability

Data will be made available on request.

Acknowledgements

The authors would like to thank Dr. Johannes Hohlbein and Dr. Antonio Aloi for their helpful comments and constructive feedback. This publication is part of the project Localbiofood (with project number 731.017.204) of the research program Science PPP Fund, which is (partly) financed by the Dutch Research Council (NWO) in collaboration with ChemistryNL. We would like to thank all our colleagues in the LocalBioFood consortium for valuable discussions.

Appendix A. Supplementary data

Supplementary data to this article can be found online at https://doi.org/10.1016/j.foodhyd.2023.109629.

References

Aguilera, J. M. (2005). Why food micro structure? *Journal of Food Engineering, 67*(1–2), 3–11. https://doi.org/10.1016/j.jfoodeng.2004.05.050

Ako, K., Durand, D., Nicolai, T., & Becu, L. (2009). Quantitative analysis of confocal laser scanning microscopy images of heat-set globular protein gels. *Food Hydrocolloids, 23*(4), 1111–1119. https://doi.org/10.1016/j.foodhyd.2008.09.003

Amatayakul, T., Halmos, A. L., Sherkat, F., & Shah, N. P. (2006). Physical characteristics of yoghurts made using exopolysaccharide-producing starter cultures and varying casein to whey protein ratios. *International Dairy Journal, 16*(1), 40–51. https://doi.org/10.1016/j.idairyj.2005.01.004

Arganda-Carreras, I., Fernández-González, R., Muñoz-Barrutia, A., & Ortiz-De-Solorzano, C. (2010). 3D reconstruction of histological sections: Application to mammary gland tissue. *Microscopy Research and Technique, 73*(11), 1019–1029. https://doi.org/10.1002/jemt.20829

Arltoft, D., Ipsen, R., Madsen, F., & de Vries, J. (2007). Interactions between carrageenans and milk proteins: A microstructural and rheological study. *Biomacromolecules, 8*(2), 729–736. https://doi.org/10.1021/bm061099q

Arltoft, D., Madsen, F., & Ipsen, R. (2007). Screening of probes for specific localisation of polysaccharides. *Food Hydrocolloids, 21*(7), 1062–1071. https://doi.org/10.1016/j.foodhyd.2006.07.020

Auty, M. A. E., Twomey, M., Guinee, T. P., & Mulvihill, D. M. (2001). Development and application of confocal scanning laser microscopy methods for studying the distribution of fat and protein in selected dairy products. *Journal of Dairy Research, 68*(3), 417–427. https://doi.org/10.1017/S0022029901004873

Berg, E. A., & Fishman, J. B. (2019). Labeling antibodies using N -hydroxysuccinimide (NHS) -fluorescein, 229–231 https://doi.org/10.1101/pdb.prot099283.

Cerning, J. (1990). Exocellular polysaccharides produced by lactic acid bacteria. *FEMS Microbiology Letters, 87*(1–2), 113–130. https://doi.org/10.1016/0378-1097(90)90701-Q

Dalgleish, D. G., & Law, A. J. R. (1988). pH-Induced dissociation of bovine casein micelles. I. Analysis of liberated caseins. *Journal of Dairy Research, 55*(4), 529–538. https://doi.org/10.1017/S0022029900033306

Doube, M., Klosowski, M. M., Arganda-Carreras, I., Cordelières, F. P., Dougherty, R. P., Jackson, J. S., et al. (2010). BoneJ: Free and extensible bone image analysis in ImageJ. *Bone, 47*(6), 1076–1079. https://doi.org/10.1016/j.bone.2010.08.023

Faber, E. J., Zoon, P., Kamerling, J. P., & Vliegenthart, J. F. G. (1998). The exopolysaccharides produced by Streptococcus thermophilus Rs and Sts have the same repeating unit but differ in viscosity of their milk cultures. *Carbohydrate Research, 310*(4), 269–276. https://doi.org/10.1016/S0008-6215(98)00189-X

Faers, M. A., Choudhury, T. H., Lau, B., Mcallister, K., & Luckham, P. F. (2006). Syneresis and rheology of weak colloidal particle gels, 288, 170–179 https://doi.org/10.1016/j.colsurfa.2006.03.031.

Fang, Y., Zhang, H., & Nishinari, K. (2021). *Food hydrocolloids: Functionalities and applications*. Springer.

Foroutanparsa, S., Brüls, M., Maljaars, C. E. P., Tas, R. P., & Voets, I. K. (2023). Spatial distribution of αs1-caseins and β-caseins in milk gels acidified with glucono-δ-lactone. *Food Hydrocolloids, 139*(August 2022), Article 108506. https://doi.org/10.1016/j.foodhyd.2023.108506

Foroutanparsa, S., Brüls, M., Tas, R. P., Maljaars, C. E. P., & Voets, I. K. (2021). Super resolution microscopy imaging of pH induced changes in the microstructure of casein micelles. *Food Structure, 30*(January), Article 100231. https://doi.org/10.1016/j.foostr.2021.100231

Girard, M., & Schaffer-Lequart, C. (2007). Gelation of skim milk containing anionic exopolysaccharides and recovery of texture after shearing. *Food Hydrocolloids, 21*(7), 1031–1040. https://doi.org/10.1016/j.foodhyd.2006.07.012

Glover, Z. J., Ersch, C., Andersen, U., Holmes, M. J., Povey, M. J., Brewer, J. R., et al. (2019). Super-resolution microscopy and empirically validated autocorrelation image analysis discriminates microstructures of dairy derived gels. *Food Hydrocolloids, 90*(September 2018), 62–71. https://doi.org/10.1016/j.foodhyd.2018.12.004

Harwalkar, V. R., & Kalab, M. (1986). Relationship between microstructure and susceptibility to syneresis in yoghurt made from reconstituted nonfat dry milk. *Food Microstructure, 5*(2), 287–294.

Hassan, A. N. (2008). ADSA foundation scholar award: Possibilities and challenges of exopolysaccharide-producing lactic cultures in dairy foods. *Journal of Dairy Science, 91*(4), 1282–1298. https://doi.org/10.3168/jds.2007-0558

Hassan, A. N., Frank, J. F., & Qvist, K. B. (2002). Direct observation of bacterial exopolysaccharides in dairy products using confocal scanning laser microscopy. *Journal of Dairy Science, 85*(7), 1705–1708. https://doi.org/10.3168/jds.S0022-0302(02)74243-4

Hassan, A. N., Frank, J. F., Schmidt, K. A., & Shalabi, S. (1996). Rheological properties of yogurt made with encapsulated nonropy lactic cultures, 2091–2097 https://doi.org/10.3168/jds.S0022-0302(96)76582-7.

Hassan, A. N., Ipsen, R., Janzen, T., & Qvist, K. B. (2003). Microstructure and rheology of yogurt made with cultures differing only in their ability to produce exopolysaccharides. *Journal of Dairy Science, 86*(5), 1632–1638. https://doi.org/10.3168/jds.S0022-0302(03)73748-5

Hell, S. W., & Wichmann, J. (1994). Breaking the diffraction resolution limit by stimulated emission: Stimulated-emission-depletion fluorescence microscopy. *Optics Letters, 19*(11), 780. https://doi.org/10.1364/ol.19.000780

Horne, D. S. (1998). *Casein interactions : Casting light on the black boxes , the structure in dairy products* (Vol. 6946, pp. 171–177), 98.

Hussain, I., Grandison, A. S., & Bell, A. E. (2012). Effects of gelation temperature on Mozzarella-type curd made from buffalo and cows' milk. 1: Rheology and microstructure. *Food Chemistry, 134*(3), 1500–1508. https://doi.org/10.1016/j.foodchem.2012.03.062

Jabermoradi, A., Yang, S., Gobes, M., Van Duynhoven, J. P., & Hohlbein, J. (2022). Enabling single-molecule localization microscopy in turbid food emulsions. *Philosophical Transactions of the Royal Society A, 380*(2220), 20200164.

Kleerebezem, M., Van Kranenburg, R., Tuinier, R., Boels, I. C., Zoon, P., Looijesteijn, E., et al. (1999). Exopolysaccharides produced by Lactococcus lactis: From genetic engineering to improved rheological properties? *Antonie van Leeuwenhoek, International Journal of General and Molecular Microbiology, 76*(1–4), 357–365. https://doi.org/10.1023/A:1002084822851

Kunji, E. R. S. (1996). The proteolytic systems of lactic acid bacteria. *Antonie van Leeuwenhoek, International Journal of General and Molecular Microbiology, 70*(2–4), 187–221. https://doi.org/10.1007/BF00395933

Laneuville, S. I., & Turgeon, S. L. (2014). Microstructure and stability of skim milk acid gels containing an anionic bacterial exopolysaccharide and commercial polysaccharides. *International Dairy Journal, 37*(1), 5–15. https://doi.org/10.1016/j.idairyj.2014.01.014

Lee, T. (1994). Building skeleton models via 3-D medial surface/Axis thinning algorithms. *Graphical Models and Image Processing, 56*(6), 462–478. https://doi.org/10.1006/gmip.1994.1043

Lee, W. J., & Lucey, J. A. (2003). Rheological properties, whey separation, and microstructure in set-style yogurt: Effects of heating temperature and incubation temperature. *Journal of Texture Studies, 34*(5–6), 515–536. https://doi.org/10.1111/j.1745-4603.2003.tb01079.x

Lee, W. J., & Lucey, J. A. (2004). Structure and physical properties of yogurt gels: Effect of inoculation rate and incubation temperature. *Journal of Dairy Science, 87*(10), 3153–3164. https://doi.org/10.3168/jds.S0022-0302(04)73450-5

Lee, W. J., & Lucey, J. A. (2010). Formation and physical properties of yogurt. *Journal of Dairy Science, 23*(9), 1127–1136. https://doi.org/10.3168/jds.S0022-0302(02)74078-2

Lucey, J. A. (2002). Formation and physical properties of milk protein gels. *Journal of Dairy Science, 85*(2), 281–294. https://doi.org/10.3168/jds.S0022-0302(02)74078-2

Lucey, J. A., Munro, P. A., & Singh, H. (1998). Whey separation in acid skim milk gels made with glucono-δ-lactone: Effects of heat treatment and gelation temperature. *Journal of Texture Studies, 29*(4), 413–426.

Mende, S., Rohm, H., & Jaros, D. (2016). Influence of exopolysaccharides on the structure, texture, stability and sensory properties of yoghurt and related products. *International Dairy Journal, 52*, 57–71. https://doi.org/10.1016/j.idairyj.2015.08.002

Modler, H. W., & Kalab, M. (1983a). Microstructure of yogurt stabilized with milk proteins. *Journal of Dairy Science, 66*(3), 430–437. https://doi.org/10.3168/jds.S0022-0302(83)81810-4

Modler, H. W., & Kalab, M. (1983b). Microstructure of yogurt stabilized with milk proteins. *Journal of Dairy Science, 66*(3), 430–437. https://doi.org/10.3168/jds.S0022-0302(83)81810-4

Ni, H., & Raikos, V. (2019). Lactic-acid bacteria fermentation-induced e ff ects on microstructure and interfacial properties of oil-in-water emulsions stabilized by goat-milk proteins. *LWT -Food Science and Technology, 109*, 70–76. https://doi.org/10.1016/j.lwt.2019.04.002

Nieuwland, M., Bouwman, W. G., Bennink, M. L., Silletti, E., & de Jongh, H. H. J. (2015). Characterizing length scales that determine the mechanical behavior of gels from crosslinked casein micelles. *Food Biophysics, 10*(4), 416–427. https://doi.org/10.1007/s11483-015-9399-y

Odgaard, A., & Gundersen, H. J. (1993). Quantification of connectivity with special emphasis on 3D reconstractions. *Bone, 14*, 173–182.

Pugnaloni, L. A., Matia-Merino, L., & Dickinson, E. (2005). Microstructure of acid-induced caseinate gels containing sucrose: Quantification from confocal microscopy and image analysis. *Colloids and Surfaces B: Biointerfaces, 42*(3–4), 211–217. https://doi.org/10.1016/j.colsurfb.2005.03.002

Rajoka, M. S. R., Mehwish, H. M., Kitazawa, H., Barba, F. J., Berthelot, L., Umair, M., et al. (2022). Techno-functional properties and immunomodulatory potential of exopolysaccharide from Lactiplantibacillus plantarum MM89 isolated from human breast milk. *Food Chemistry, 377*(December 2021), Article 131954. https://doi.org/10.1016/j.foodchem.2021.131954

Riaz Rajoka, M. S., Wu, Y., Mehwish, H. M., Bansal, M., & Zhao, L. (2020). Lactobacillus exopolysaccharides: New perspectives on engineering strategies, physiochemical functions, and immunomodulatory effects on host health. *Trends in Food Science and Technology, 103*(July), 36–48. https://doi.org/10.1016/j.tifs.2020.06.003

Robertson, C. (2012). Theory and practical recommendations for autocorrelation-based image correlation spectroscopy. *Journal of Biomedical Optics, 17*(8), Article 080801. https://doi.org/10.1117/1.jbo.17.8.080801

Roefs, S. P. F. M., De Groot-Mostert, A. E. A., & Van Vliet, T. (1990). Structure of acid casein gels 1. Formation and model of gel network. *Colloids and Surfaces, 50*(C), 141–159. https://doi.org/10.1016/0166-6622(90)80259-7

Ruas-Madiedo, P., Alting, A. C., & Zoon, P. (2005). Effect of exopolysaccharides and proteolytic activity of Lactococcus lactis subsp. cremoris strains on the viscosity and structure of fermented milks. *International Dairy Journal, 15*(2), 155–164. https://doi.org/10.1016/j.idairyj.2004.05.009

Silva, J. V. C., Legland, D., Cauty, C., Kolotuev, I., & Floury, J. (2015). Characterization of the microstructure of dairy systems using automated image analysis. *Food Hydrocolloids, 44*, 360–371. https://doi.org/10.1016/j.foodhyd.2014.09.028

Teggatz, J., & Morris, H. A. (1990). Changes in the rheology and microstructure of ropy yogurt during shearing. *Food Microstructure, 9*(2), 133–138.

Tiwari, S., Kavitake, D., Devi, P. B., & Halady Shetty, P. (2021). Bacterial exopolysaccharides for improvement of technological, functional and rheological properties of yoghurt. *International Journal of Biological Macromolecules, 183*, 1585–1595. https://doi.org/10.1016/j.ijbiomac.2021.05.140

Tuinier, R., ten Grotenhuis, E., Holt, C., Timmins, P. A., & de Kruif, C. G. (1999). Depletion interaction of casein micelles and an exocellular polysaccharide. *Physical Review E - Statistical Physics, Plasmas, Fluids, and Related Interdisciplinary Topics, 60*(1), 848–856. https://doi.org/10.1103/PhysRevE.60.848

Urban, N. T., Willig, K. I., Hell, S. W., & Nägerl, U. V. (2011). STED nanoscopy of actin dynamics in synapses deep inside living brain slices. *Biophysical Journal, 101*(5), 1277–1284. https://doi.org/10.1016/j.bpj.2011.07.027

Van den Bijgaart, H. J. C. M. (1988). *Syneresis of rennet-induced milk gels as influenced by cheesemaking parameters*. Wageningen University and Research.

van Vliet, T., van Dijk, H. J. M., Zoon, P., & Walstra, P. (1991). Relation between syneresis and rheological properties of particle gels. *Colloid & Polymer Science, 269* (6), 620–627. https://doi.org/10.1007/BF00659917

Zhang, L., Folkenberg, D. M., Amigo, J. M., & Ipsen, R. (2016). Effect of exopolysaccharide-producing starter cultures and post-fermentation mechanical treatment on textural properties and microstructure of low fat yoghurt. *International Dairy Journal, 53*, 10–19. https://doi.org/10.1016/j.idairyj.2015.09.008

Zhang, L., Folkenberg, D. M., Qvist, K. B., & Ipsen, R. (2015). Further development of a method for visualisation of exopolysaccharides in yoghurt using fluorescent conjugates. *International Dairy Journal, 46*, 88–95. https://doi.org/10.1016/j.idairyj.2014.08.018